Limits on superconductivity-related magnetization in Sr_2RuO_4 and $PrOs_4Sb_{12}$ from scanning SQUID microscopy

Clifford W. Hicks,[1,2] John R. Kirtley,[3] Thomas M. Lippman,[1,3] Nicholas C. Koshnick,[3] Martin E. Huber,[4] Yoshiteru Maeno,[5] William M. Yuhasz,[6] M. Brian Maple,[7] and Kathryn A. Moler[1,3]

[1]*Stanford Institute for Materials and Energy Sciences, SLAC National Accelerator Laboratory, 2575 Sand Hill Road, Menlo Park, California 94025, USA*
[2]*School of Physics and Astronomy, University of St Andrews, St Andrews KY16 9SS, United Kingdom*
[3]*Geballe Laboratory for Advanced Materials, Stanford University, Stanford, California 94305, USA*
[4]*Departments of Physics and Electrical Engineering, University of Colorado Denver, Denver, Colorado 80217, USA*
[5]*Department of Physics, Graduate School of Science, Kyoto University, Kyoto 606-8502, Japan*
[6]*Division of Materials Sciences and Engineering, Ames Laboratory, Ames, Iowa 50011, USA*
[7]*Department of Physics, University of California–San Diego, La Jolla, California 92093, USA*

We present scanning superconducting quantum interference device microscopy data on the superconductors Sr_2RuO_4 ($T_c=1.5$ K) and $PrOs_4Sb_{12}$ ($T_c=1.8$ K). In both of these materials, superconductivity-related time-reversal symmetry-breaking fields have been observed by muon spin rotation; our aim was to visualize the structure of these fields. However, in neither Sr_2RuO_4 nor $PrOs_4Sb_{12}$ do we observe spontaneous superconductivity-related magnetization. In Sr_2RuO_4, many experimental results have been interpreted on the basis of a $p_x \pm ip_y$ superconducting order parameter. This order parameter is expected to give spontaneous magnetic induction at sample edges and order parameter domain walls. Supposing large domains, our data restrict domain wall and edge fields to no more than ~0.1% and ~0.2% of the expected magnitude, respectively. Alternatively, if the magnetization is of the expected order, the typical domain size is limited to ~30 nm for random domains or ~500 nm for periodic domains.

I. INTRODUCTION

Sr_2RuO_4 is a highly two-dimensional (2D), layered perovskite superconductor with $T_c \approx 1.5$ K in the clean limit. Its in-plane coherence length is $\xi_{ab}(0)=66$ nm (Ref. 1) and magnetic penetration depth $\lambda_{ab}=160–190$ nm.[2–4] On the Fermi sheet thought to be dominant for superconductivity (the γ sheet), the electron mass is $16m_e$ (5.5 times the band mass).[1] $PrOs_4Sb_{12}$ is a heavy fermion superconductor of cubic symmetry, with m^* in the range of tens of m_e.[5,6] Measurements of specific heat show an unusual double superconducting transition, with $T_{c1} \approx 1.86$ K and $T_{c2} \approx 1.70$ K.[7–9] The coherence length of $PrOs_4Sb_{12}$ is $\xi=12$ nm, while muon spin rotation (μSR) measurements yield $\lambda(0) \approx 350$ nm.[10,11]

Sr_2RuO_4 and $PrOs_4Sb_{12}$ both have unusual superconducting states. Strong evidence for either line nodes or deep gap minima, or both, in Sr_2RuO_4 comes from, e.g., rf,[12] microwave,[2] and specific heat measurements.[13,14] In $PrOs_4Sb_{12}$, rf and thermal conductivity measurements suggest point nodes[15] while μSR and Sb nuclear quadrupole resonance (NQR) show fully gapped superconductivity (at ambient pressure).[10,11,16] Nodes may exist on a small-gap band suppressed by modest applied fields.[11] Additional thermal conductivity measurements confirm multiband superconductivity but indicate no nodes on either gap.[17] In Sr_2RuO_4, specific heat measured against applied field confirms multiband superconductivity,[13] and that if not nodes there are at least deep minima on the primary band.

Triplet pairing has been shown in Sr_2RuO_4 with high certainty by measurement of the ^{17}O Knight shift.[18] Measurement of the muon Knight shift in $PrOs_4Sb_{12}$ also indicates

triplet pairing but with less certainty: owing to low-lying crystal electric field states, the expected Knight shift for singlet pairing is less clear.[19]

The absence of a Hebel-Slichter peak in Ru NMR measurements on Sr_2RuO_4 (Ref. 20) and in Sb NQR measurements on $PrOs_4Sb_{12}$ (Refs. 16 and 21) indicate unconventional superconductivity in both materials. In Sr_2RuO_4, it is confirmed by demonstration that $T_c \rightarrow 0$ as the mean free path shrinks to $\sim \xi_{ab}$.[22] In $PrOs_4Sb_{12}$, T_{c1} shows a modest, and T_{c2} possibly a more pronounced, sensitivity to sample quality.[7] Odd-parity orbital symmetry in Sr_2RuO_4 has been shown by fabrication of a π-SQUID,[23] and superconductivity-related time-reversal symmetry breaking (TRSB) by measurement of the Kerr effect.[24] A two-component order parameter is indicated by Josephson interferometry,[25] hysteretic transport in microstructures,[26] and a jump in the transverse sound velocity at T_c.[27] These results have all been interpreted in terms of a chiral $p_x \pm ip_y$ orbital order parameter. The order parameter of $PrOs_4Sb_{12}$ remains an open question; possibilities for both singlet and triplet pairing are listed in Ref. 28.

Along with the shared features described above, Sr_2RuO_4 and $PrOs_4Sb_{12}$ are also the only two materials where observation of spontaneous, superconductivity-related TRSB fields by μSR is well established. In Sr_2RuO_4, an average internal induction far below T_c of ~0.5 G is found, with the rapid initial decay of muon polarization indicating a peak induction of at least ~5 G,[4,29] indicating a dilute density of sources. In $PrOs_4Sb_{12}$, the average internal induction is at least twice as large, ~1.5 G (Ref. 30) but its distribution is not as peaked as in Sr_2RuO_4, suggesting a higher source

density. The TRSB appears to onset at the upper transition (~1.85 K).

For $p_x \pm ip_y$ order in Sr_2RuO_4, a magnetization along the z axis (crystalline c axis) is expected: the orbital angular momentum of the condensate would give an uncanceled current at domain edges (meaning domain walls and sample edges). Inward from these edges, Meissner screening would in turn result in counterflowing screening currents. If each pair in the γ-sheet condensate is assigned angular momentum $\hbar$, an edge current of $k_F^2 \hbar e / 8\pi m^* = 2.6$ μA per layer results,[31] for a field discontinuity of 50 G. Matsumoto and Sigrist (MS) have solved the Bogoliubov-de Gennes equations in a quasi-classical approximation for an ideal $p_x \pm ip_y$ superconductor (without secondary bands or gap minima/nodes, and with specular scattering at edges) and obtain edge and domain wall inductions peaking at ~10 G and ~20 G, respectively.[32] (We scale their unitless results by $\xi = 66$ nm and $\lambda_L = 165$ nm; they assume $\lambda_L / \xi = 2.5$.)

There is conflicting experimental guidance on domain size: Kerr rotation indicates domains at least a few times larger than the beam size, or $\gtrsim 100$ μm (Ref. 24), while Josephson interferometry suggests domains at the edges ~1 μm across.[25] The π-SQUID required phase coherence across the 0.6 mm width of the Sr_2RuO_4 crystal, indicating large domains.[23] If the MS result is approximately correct (i.e., a ~10 G field across a width $\sim 2\lambda_{ab}$ at domain walls), the 0.5 G average internal field observed by μSR suggests ~10 μm domains. Domain size might be affected by the cooling rate through T_c, which was ~1 K/h for the Kerr, Josephson interferometry, and π-SQUID experiments, and faster for the μSR measurement. Domain size is discussed in more detail in Ref. 33.

To date, edge and domain wall fields have not been observed by scanning magnetic probes in Sr_2RuO_4. Scanning Hall probe measurements by Björnsson *et al.* constrain edge and domain wall currents to be less than ~3% and 8% of the MS results, respectively.[34,35] [The scan area was (70 μm)^2 so domain walls may have been absent.] Kirtley *et al.*, in SQUID scans spanning a ≈ 1-mm-wide sample, improve the limit on both edge and domain wall currents to about 1% of the expectation, for domains larger than ~8 μm.[35]

Analysis by Ashby and Kallin show that nonspecular or pair-breaking edge scattering could reduce the expected edge magnetization, but not by the orders of magnitude required for consistency with experiment.[36] Selection of Ginzberg-Landau (GL) parameters nearer the edge of stability for $p_x + ip_y$ order reduces the edge currents but also spreads them out over a larger range, so the total flux, and the observed signal in scanning probes microns above the surface, would not be greatly reduced.

The work here further tightens the limits on chiral currents and domain structure in Sr_2RuO_4. We also discuss the possibility of periodic domains and show the first magnetic scans of $PrOs_4Sb_{12}$.

II. MAGNETIC SCANS OF Sr_2RuO_4

The scanning SQUID used here is a niobium-based device, described in Refs. 37 and 38. Flux is coupled into the
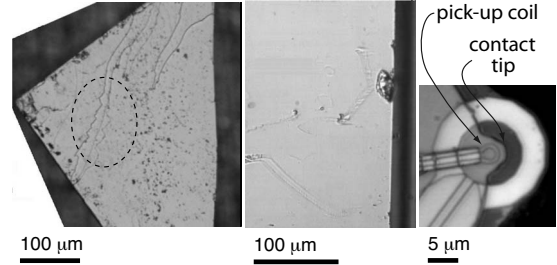

FIG. 1. Left: photograph of the Sr_2RuO_4 sample scanned in this work. The surface is a cleaved *ab* surface. The left edges are polished and the right is a growth edge. Cleave terraces visible in the magnetic scans are circled. Middle: $PrOs_4Sb_{12}$. The right edge is a growth edge. Right: front end of the SQUID used in this work. The pick-up coil (of diameter 3.2 μm) and contact tip, the point where the SQUID contacts the sample, are indicated.

SQUID through a 3.2-μm-diameter pick-up coil (Fig. 1). The leads to the pick-up coil are shielded to minimize flux coupling into the space between the leads. SQUIDs are flux-sensitive devices, so the units on the data shown in this work are units of flux; 1 $\Phi_0 \equiv hc/2e$ in a 3.2 μm loop corresponds to an average induction of ≈ 2.5 G. The SQUID was generally scanned on a plane ~1 μm out of contact with the sample, to reduce noise and spurious features from surface roughness.

The Sr_2RuO_4 crystal (photograph: Fig. 1) was grown in a floating-zone furnace and was not annealed after growth.[39] All scans were done at $T = 0.4$ K, with fairly rapid cooling through T_c, ~1 K/min. For the mosaic of scans shown in
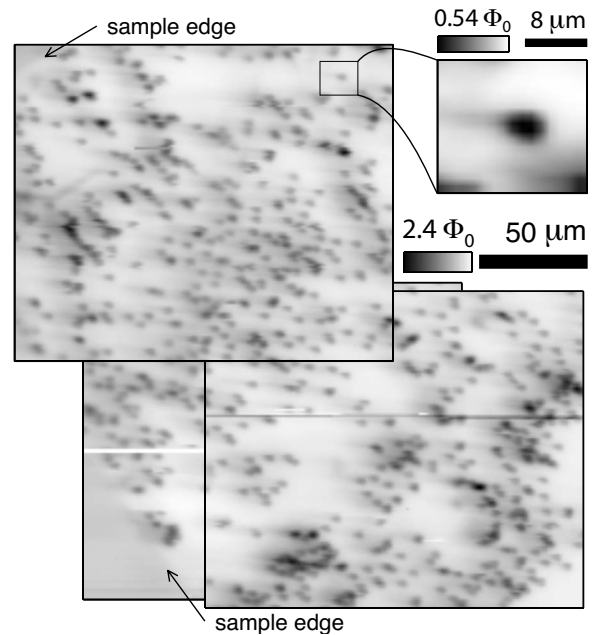

FIG. 2. Three overlapping SQUID magnetometry scans of the Sr_2RuO_4 crystal pictured in Fig. 1, in earth's ~1/2 Oe field. Single vortices are clearly visible. Across the entire scan range, vortices are lined up along upper-left-to-lower-right stripes. A closeup of a single vortex is shown at the upper right; the weak tail extending leftward from the vortex is an artifact of the SQUID imaging kernel.

Fig. 2, the crystal was cooled in earth's ∼1/2 Oe field with the out-of-plane component canceled by ∼50% by an applied field; however the applied field was subsequently turned off and vortices reintroduced into the sample, to approximately match the ambient field, by electromagnetic noise from the positioners. The weak tails that extend leftward from each vortex, clearly visible in the closeup of a single vortex, are artifacts of the imaging kernel: the shielding of the pick-up coil leads is not perfect. The full extent of these tails can be seen in Fig. 6(c): ∼70 μm, about the distance between the pick-up coil and the point where the shielding becomes a fully formed coaxial cable.

Although not the main point of this paper, the mixed-state scans of Fig. 2 contain three features worth noting. (1) The local vortex distribution is uneven. Even at small applied fields, where direct vortex-vortex interaction is negligible, minimization of global field energy encourages a homogeneous vortex density—compare with the much more homogeneous vortex distribution in clean areas of $PrOs_4Sb_{12}$, at an applied field of 760 mOe [Fig. 6(a)]. Local vortex coalescence has been previously reported in Sr_2RuO_4,[34,40,41] and also in MgB_2, where it was explained as originating from the two-component order parameter, one in the type-II regime, and the other type-I.[42] As Sr_2RuO_4 is only weakly type-II [$\kappa_{ab}=\lambda_{ab}(0)/\xi_{ab}(0)\approx2.6$; $\kappa>1/\sqrt{2}$ indicates type-II] and has a two-component order parameter, the cause of local clustering might be similar. (2) The large-scale distribution is also uneven: toward the lower right and upper left, vortex-free areas up to ∼30 μm across are adjacent to similar-sized regions of high vortex density. These regions may indicate spatially-varying sample quality. (3) The distribution is anisotropic: over the entire ≈300-μm-wide scan area, vortices line up along upper-left-to-lower-right stripes. A striped vortex distribution was also reported in Ref. 34. In highly anisotropic superconductors, c-axis vortices can form chains along in-plane vortices, a phenomenon that has been observed in Sr_2RuO_4.[43] However, an in-plane field of ∼10 Oe appears to be required to form and orient well-defined chains,[40] whereas the field for Fig. 2 was no more than earth's ∼1/2 Oe, and ∼50 mOe in Ref. 34.

Figure 3 shows this paper's main results on Sr_2RuO_4: magnetic scans in the near absence of vortices. The scans overlap, however each is a separate thermal cycle (to above T_c). Four prominent features appear in the scans: (1) in panel (a), there are two vortices, one at the lower left and the other beyond the right edge of the scan. (The extended dipole-like feature is part of its tail.) (2) The step changes in the signal across cleave terraces and the sample edge result from SQUID-sample interaction, not static magnetization: the SQUID is scanned on a plane ∼1 μm above the sample surface, so when the pick-up coil passes over topographic features its proximity to the sample changes. In operation, the SQUID is biased with a dc voltage and the current, which varies with the SQUID's critical current, is measured. Changing the proximity between the pick-up coil and a metallic surface affects the inductance of that arm of the SQUID, which in turn affects the critical current (as does varying flux in the SQUID, the desired signal).[44] (3) An edge shadow, the blurred dark line in panels (b) and (c), is also an artifact. It appears to correspond to a step change in magnetic
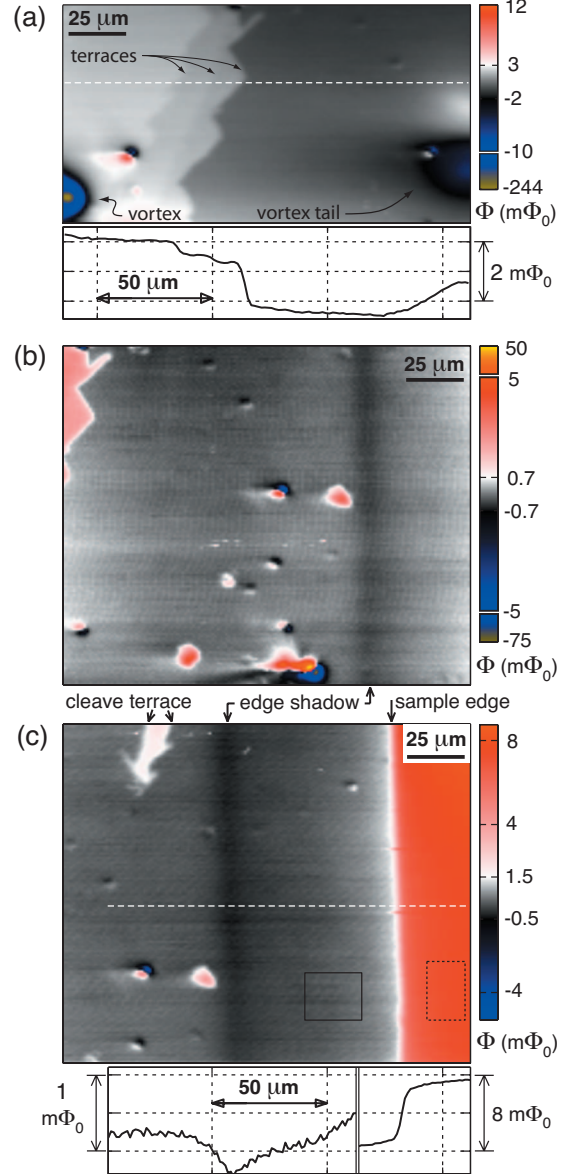

FIG. 3. (Color) Overlapping scans of Sr_2RuO_4 at 0.4 K; each is a separate thermal cycle. In none of these three scans does the spontaneous edge and domain-wall magnetization expected from chiral superconductivity appear. (a) A scan over the cleave terraces, of total height ∼700 nm, indicated in Fig. 1(a), and (lower panel) a section along the dashed line. Note the broken color scale: the peak vortex signal far exceeds all other features. The terrace signal is an artifact of SQUID-sample interaction. The vortex tail, from a vortex ∼50 μm beyond the right edge of the scan, is an imaging kernel artifact. (b) An area with fewer terraces. The "edge shadow" is an imaging kernel artifact. Other features include dipoles (magnetic inclusions) and some terraces. (c) A scan over the sample edge and (lower panel) a section along the dashed line. The rms signal in the solid and dotted boxes, after local plane subtraction, are 0.06 $m\Phi_0$ and 0.05 $m\Phi_0$, respectively.

field across the sample edge, with the ∼70 μm distance between the shadow and the edge being set by the far extent of the SQUID imaging kernel, i.e., the tails discussed above. (4) There are numerous magnetic dipoles, most very weak: compare their signals with that from the vortices. The source of

the dipoles was not investigated, however typical dipoles in the scans, with peak signals of $0.1-5$ mΦ_0, could be accounted for by inclusions of SrRuO$_3$, a ferromagnet with $1.6-2$ μ_B/Ru,[45] $\sim 20-80$ nm on a side. (Tails on some of the dipoles, like the vortex tails, are imaging kernel artifacts.)

III. ABSENCE OF OBSERVED SPONTANEOUS MAGNETIZATION IN Sr$_2$RuO$_4$

No edge or domain wall magnetization, expected for $p_x \pm i p_y$ order, is apparent in the Sr$_2$RuO$_4$ scans. To compare this null result with theoretical expectation, it is necessary to account for the finite sensor resolution and scan height. We model the pick-up coil as a 3.2-μm-diameter wire loop parallel to the surface, with perfect coupling of B_z inside and zero outside. Empirical scan heights consistent with this model are obtained by studying the vortex and dipoles in Fig. 3: For scan heights much larger than λ_{ab}, the field distribution of a vortex approaches that of a monopole placed a depth λ_{ab} beneath the surface. The vortex in Fig. 3(a) has a full width at half maximum (FWHM) (along y) of 3.8 μm and a peak signal of 0.25 Φ_0. In the monopole model, these values correspond to heights above the monopole of 1.6 μm and 1.9 μm, respectively, or, subtracting λ, ≈ 1.6 μm above the sample surface. Heights above the dipoles are obtained by fitting the 2D scan data to the simulated response from a pointlike dipole, with dipole strength, dipole orientation, and scan height as free parameters. The very prominent dipole near the bottom of Fig. 3(b) gives a height of 1.7 μm. Fits to two other dipoles in Fig. 3(b) give heights around 1.5 μm, and to two dipoles in Fig. 3(a), a few 0.1 μm higher. In the Sr$_2$RuO$_4$ scans, the scan height above the surface is $z \approx 1.5$ μm.

The MS calculation gives the magnetic induction deep beneath the upper surface of the sample. We extend their results to the space above the sample following the procedure in Refs. 35 and 46. If the source inductions within the superconductor are along z, then

$$\tilde{B}_z(\mathbf{k}, z) = \frac{K}{k + K} \tilde{B}_{0,z}(\mathbf{k}) e^{-kz}, \qquad (1)$$

where $K = \sqrt{k^2 + (1/\lambda_{ab})^2}$, $\tilde{B}_z(\mathbf{k})$ is the Fourier transform of $B_z(\mathbf{x})$, and z is the height above the sample surface. The $K/(k+K)$ prefactor arises from Meissner screening: at $z \gg \lambda$, its effect is that the field distribution at height z is what it would be at $z + \lambda$ without the prefactor. We obtain the expected signal at edges and domain walls by applying Eq. (1), with $\lambda_{ab} = 190$ nm, to the MS results, then averaging over a 3.2-μm-diameter circle. [The accounting of Meissner screening in Eq. (1) is correct over featureless surfaces. However we apply Eq. (1) to edges, too: the error on z exceeds λ so this is a secondary error that does not affect our conclusions.] Comparisons of expected and observed signals are shown in Fig. 4. The expected signal is shown for $z = 1.5$ μm, however the choice of z is not critical: a doubling of z reduces expected edge signals by $\sim 30\%$ and domain wall signals by $\sim 60\%$.
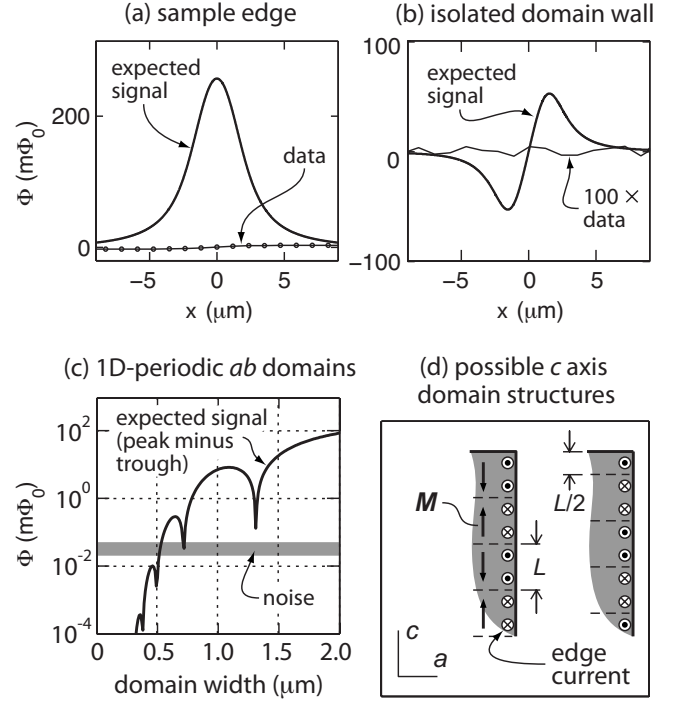

FIG. 4. (a)–(c) Expected signals compared with observed data on Sr$_2$RuO$_4$ for (a) a sample edge, (b) an isolated domain wall, and (c), domains periodic along one direction in the ab plane. The expected signals were obtained by extension of the MS results to a scan height of 1.5 μm, using Eq. (1), followed by averaging over a 3.2-μm-diameter pick-up coil. The data in (a) and (b) is along the dashed line in Fig. 3(c), and the noise level indicated in (c) is the pixel-to-pixel noise in the boxes in Fig. 3(c). (d) Hypothetical c-axis domain structures with the magnetization direction and equivalent edge currents indicated. Taking $|\mathbf{M}| = 10$ G, for the cases at left and right our scans indicate $L < 20$ nm and 400 nm, respectively.

Figures 5(a) and 5(b) show simulated scans, taking $z = 2$ μm (the upper bound of the actual scan height), for particular configurations of domains averaging 15 μm and 2 μm across, respectively. The domains are quasiperiodic for computational convenience; their rms area variation is 38% of the mean. In panel (d), the simulated scans multiplied by a scale factor are added to the observed signal. For domains 2 μm and larger, domain wall fields would have been visible at $\sim 0.1\%$ of the MS result. To look at edge fields separately, in (e) the edge fields alone of the simulation are added to the data. Weak edge fields appear as modulations of the shape of the step, and would have been visible at $\sim 0.2\%$ of the expectation for 4 μm or larger domains, or $\sim 1\%$ for 2 μm domains.

We cannot definitively exclude the possibility that the entire sample is a single domain, and the edge signal is merged with the 6 mΦ_0 step at the sample edge (due to SQUID-sample interaction). In this case, the limit on the edge signal is ~ 6 mΦ_0 or $\sim 3\%$ of the expectation. However, we note again that the 0.5 G induction observed by μSR is a volume average: it is highly unlikely that its source is entirely excluded from our $\sim (150$ μm$)^2$ scan area.

How large could domains be if they were completely random? For random domains magnetized along $\hat{\mathbf{z}}$, the expected
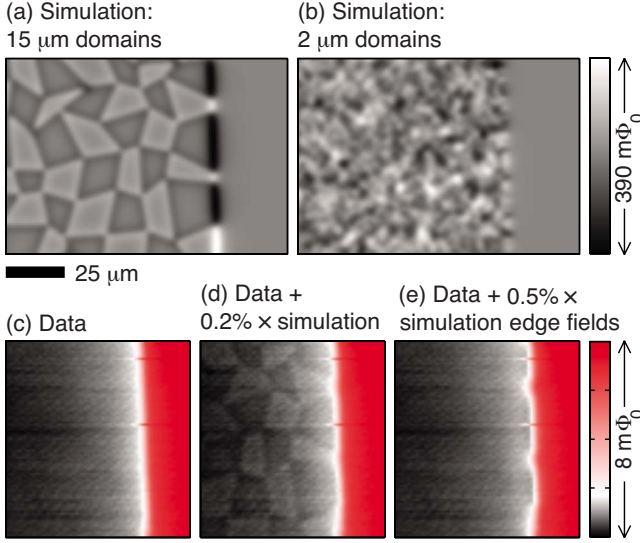
FIG. 5. (Color online) (a) and (b) Simulated scans of a quasiperiodic domain structure in Sr_2RuO_4. The MS results are extended to $z=2.0$ μm using Eq. (1), then averaged over a 3.2-μm-diameter pick-up coil. (c) Observed signal, from Fig. 3(c). (d) and (e) Observed signal plus a scale factor times the simulation. In (e), domain-wall contributions are removed.

field at scan height z is given by Eq. 15 of Ref. 46,

$$\langle B_z^2 \rangle = \frac{15\pi}{2} \frac{\lambda^3}{(z+\lambda)^6} M^2 V, \qquad (2)$$

where M is the typical magnetization and V typical domain volume. B_z would vary on a length scale $\sim z$; here z is comparable to the pick-up coil radius so the signal is $\sim B_z z^2$. The observed signal over a featureless area of the sample is 0.06 mΦ_0 rms [see Fig. 3(c)], and over a section of vacuum, 0.05 mΦ_0 rms. Taking $z=2$ μm, obtaining a signal less than 0.02 mΦ_0 with $M=10[1]$ G requires $V<(6\text{ nm})^3$ $[<(30\text{ nm})^3]$.

Larger domains are not excluded if they are periodic. Figure 4(c) shows the expected signal from domains periodic along one direction in the ab plane, taking the MS result for the domain-wall magnetization. Domains perfectly periodic along a could have been as wide as ~ 0.5 μm without being detected.

Domains could also be periodic along c. To estimate a limit on c-axis domain widths, we take $\mathbf{M}=(0,0,\pm M)$ everywhere, with M constant; i.e., the magnetization is equivalent to thin sheet currents at the sample edge. Meissner screening does not strongly affect the field distribution for domain thicknesses $L\ll\lambda$, and so is neglected. Two possibilities for c-axis periodic domains are illustrated in Fig. 4(d). If the domains are all of equal thickness L, then the upper half of the top domain gives a far-field $|B|$ linear in L. (All remaining edge current is incorporated into alternating dipoles.) If $|M|$ is 10 G, then for a 3.2-μm-diameter pick-up coil at heights $z=1$, 1.5, and 2 μm, $L=0.02$ μm gives peak edge signals of 2.5 mΦ_0, 1.8 mΦ_0, and 1.5 mΦ_0, respectively. Alternatively, if the thickness of the top domain is halved the long-range field scales as L^2. For $L=0.40$ μm and

$z=1$, 1.5, and 2 μm, the peak edge signal is expected to be ≈ 3.8 mΦ_0, 2.3 mΦ_0, and 1.5 mΦ_0 (in the absence of Meissner screening, which would reduce the signal somewhat further).

A brief summary on the limits on chiral currents and domain sizes in Sr_2RuO_4: (1) for domains of $p_x\pm ip_y$ order larger than 2 μm across, domain-wall currents are at most $\sim 0.1\%$ of the expectation (as calculated by MS). Edge currents are at most $\sim 0.2\%$ of expectation for 4 μm and larger domains, and $\sim 1\%$ for 2 μm domains. (2) If domain wall currents are of the expected magnitude and domains are perfectly periodic stripes in the ab plane, the domain width can be up to ~ 0.5 μm (periodicity 1 μm). (3) If $|\mathbf{M}|\sim 10$ G [1 G] and the domains are random, their volume is atmost $\sim (6\text{ nm})^3$ [$\sim (30\text{ nm})^3$]. (4) If $|\mathbf{M}|\sim 10$ G and $\mathbf{M}$ is periodic along c, the domain width can be up to ~ 20 nm if all domains are of the same width or ~ 400 nm if the top domain is half the width of the others, to give an edge signal $\lesssim 1$ mΦ_0.

If a reason were found for chiral edge and domain-wall currents to be vastly less than the MS result, then a separate explanation for the source of the μSR signal would be required.

IV. MAGNETIC SCANS OF PrOs$_4$Sb$_{12}$

As with Sr_2RuO_4, in anticipation of possible edge currents a scan area of the $PrOs_4Sb_{12}$ sample extending over an edge was selected. Scans of the mixed state under $H<1$ Oe are shown in Fig. 6. [The edge is of a deep trench rather than the sample edge; a spread-out vortex, far beneath the SQUID, appears at the lower right of Fig. 6(c).] Also as with Sr_2RuO_4, the cooling rate through T_c was ~ -1 K/min.

The vortices clustered strongly at extended sample defects, the more prominent of which are visible in the photograph. Where the sample is relatively free of defects [the lower right portion of Fig. 6(a)], the vortex distribution is homogeneous, in contrast to Sr_2RuO_4.

A few opposite-sign vortices appear in panel (b), where the cooling field was 160 mOe, and in the same area of a 300 mOe scan. They do not appear in panel (c), where the cooling field was near zero, and so are not due to a magnetic inclusion. They may be a consequence of trapping of positive-sign vortices combined with overall flux expulsion: the vortex density in the 760 mOe scan approximately matches the cooling field but a significant portion of the flux was expelled in the 160 mOe scan (even after accounting for the nonzero background field).

Like the cleave terraces in Sr_2RuO_4, surface defects appear clearly in the nearly vortex-free scan [Fig. 6(c)] as a result of SQUID-sample interaction. This is proved by reversing the SQUID bias: the surface defect signal changes sign whereas the edge shadow, resulting from static magnetic fields at the edge, does not (Fig. 7).

The scan height over the $PrOs_4Sb_{12}$ sample can be determined by studying a few vortices, as in Sr_2RuO_4. The isolated vortex in Fig. 6(c) has a FWHM of 3.8 μm and a peak signal of 0.30 Φ_0, giving scan heights (above the monopole) in the monopole model of 1.6 μm and 1.5 μm, respectively,

(a) edge ↓ $H_a =$ 760 mOe

3.4 Φ_0

50 μm

(b) $H_a =$ 160 mOe

2.0 Φ_0

50 μm

(c) $H_a =$ 19 mOe (cancels bckgnd.)

300
5

Φ (mΦ_0)
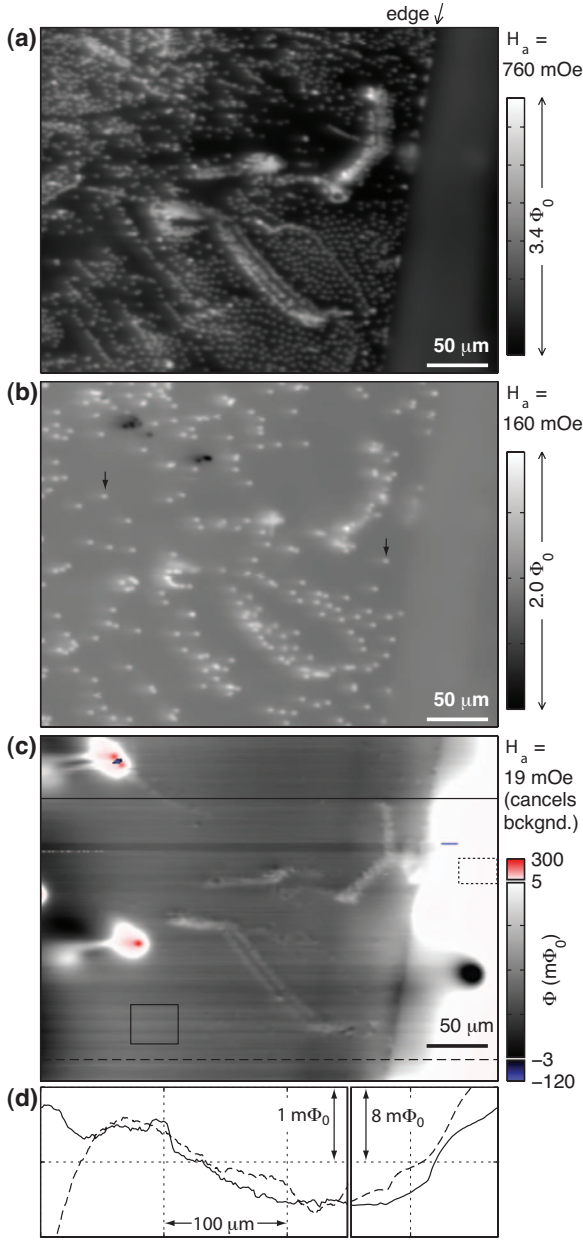
50 μm

−3
−120

(d) 1 mΦ_0 8 mΦ_0

−100 μm−

FIG. 6. (Color) (a)–(c) Magnetic scans of the PrOs$_4$Sb$_{12}$ sample shown in Fig. 1. All scans are at 0.4 K, under different cooling fields, H_a. Vortices cluster at extended defects. The indicated vortices in (b) are used for scan height determination. In (c), H_a = 19 mOe cancels the background z-axis field. Four vortices remain toward the left side of the scan and a fifth in a deep trench on the right side. Note the broken color scale: the vortex signal greatly exceeds other features. Away from the vortices, surface defects appear as an artifact of SQUID-sample interaction. A shadow ~70 μm left of the edge is an artifact of the imaging kernel and the edge. No magnetic features appear that could explain the ~1.5 G internal induction observed by μSR. After local plane subtraction, the rms signal in the solid box is 11 mΦ_0, and in the dotted box, 10 mΦ_0. (d) Sections along the solid and dashed lines in (c).

or, subtracting λ, $z \approx 1.3$ μm. The indicated vortices in panel (b) yield $z \approx 0.9$ and 1.0 μm, or ≈0.5 μm lower than in the Sr$_2$RuO$_4$ scans.

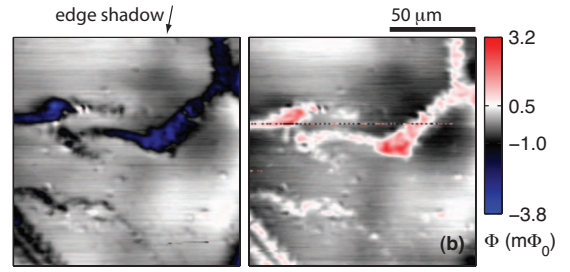edge shadow ↓   50 μm

3.2

0.5
−1.0

−3.8

(b) Φ (mΦ_0)

FIG. 7. (Color) Scans of the same area of PrOs$_4$Sb$_{12}$, with the SQUID bias current reversed between the two scans. Features resulting from SQUID-sample interaction change sign while features resulting from static magnetic inductions do not.

At a similar level to Sr$_2$RuO$_4$, no superconductivity-related TRSB fields are visible in the PrOs$_4$Sb$_{12}$ scans. Applying Eq. (2), for the case of random magnetic domains, with $M=1$ G, $\lambda=0.35$ μm, and $z=1$ μm, a signal of less than 0.1 mΦ_0 implies domains of volume less than $(30$ nm$)^3$. The lower scan height allows a somewhat tighter limit on periodic domains than in Sr$_2$RuO$_4$: if the domain magnetization is comparable to the MS result, the upper limit on domain width is ~0.4 μm.

V. DISCUSSION AND CONCLUSIONS

Reference 36 discusses the possibility that domain-wall fields in line with expectation account for the μSR data while edge fields are sharply reduced. Two mechanisms to achieve this are discussed: pair-breaking edge scattering combined with a balancing of Ginzberg-Landau parameters, and a competing edge order. If the induction observed by μSR is from domain walls, however, then as discussed above it is unlikely that observable domain walls would have been absent from the scans here and in Ref. 35. Mechanisms that might eliminate edge *and* domain-wall fields while maintaining $p_x \pm i p_y$ order include a balancing of GL parameters such that the p_x and p_y components are everywhere nearly equal,[47] or the effects of multiple bands, or nodes/deep gap minima, or strong spin-orbit coupling.[48] However, the origin of the TRSB fields observed in μSR would be left unexplained. Reference 30 discusses, in regards to PrOs$_4$Sb$_{12}$, the possibility of a finite hyperfine field induced at the μ^+ sites, which would require a nonunitary order parameter. Nonunitary pairing under $H=0$ has not been confirmed in any material, however, and is considered unlikely for Sr$_2$RuO$_4$.[1] Magnetization through pair breaking at impurity sites is not likely to be the source of the μSR signal: observable magnetization did not appear at defect sites, of which there must have been very many, across a ~100 μm range, in the scans here. Also, μSR data on a lower-T_c sample, with more defects, indicate weaker, not stronger, TRSB fields.[4]

As described above, random static domains of magnetization consistent with the μSR data would need to be on a scale ~ξ or smaller to have evaded detection. It seems unlikely that domains of an orbital order parameter could be so small. Also, in Sr$_2$RuO$_4$, the field distribution observed by μSR is more consistent with dilute sources than dense random magnetization.

The limits on periodic domains are less severe. If edge currents are of the predicted order (accounting for the μSR data), then the most plausible scenario described here for eliminating long-range edge fields may be domain periodicity along the c axis. If the periodicity is good then the domains could be up to ~ 400 nm $\sim 100 \xi_c$ in width, implying an energy cost below 1% of the condensation energy.

Closely spaced c-axis domain walls extending throughout the sample are not ruled out by experiments to date: if the structure of a domain wall is such that one of k_x or k_y remains finite across the wall, then by slow cooling it may be possible to obtain one of k_x or k_y finite throughout the crystal—domain formation may be controlled by dynamics near T_c, where ξ is longer and domain walls may interact more strongly—which would permit fabrication of π-SQUIDs.[23] Also, supposing, e.g., that k_x is the dominant component, a natural dichotomy, as observed,[25] would arise in Josephson interferometry, between junctions along the face $\perp \hat{\mathbf{x}}$, where the phase would be constant across the face, and $\perp \hat{\mathbf{y}}$, where it would alternate on a tight length scale.

However, the energetics that would drive c-axis domain formation are not clear: Meissner screening of the $k_x \pm i k_y$ edge currents cancels the long-range fields that encourage domain formation in conventional ferromagnets. Also, the absence of magnetization at microscopic surface features, such as cleave terraces, implies a tighter limit on c-axis domain width than ~ 400 nm. c-axis domains should be considered a possibility rather than a likelihood.

There is less experimental guidance on the possibilities for $PrOs_4Sb_{12}$. Because $PrOs_4Sb_{12}$ is cubic, if the orbital order parameter turns out to break time-reversal symmetry then a more complex domain structure than in Sr_2RuO_4 is expected.[49] For example, in Ref. 28, a singlet order $\sim (d_{yz} + id_{xz} + 0d_{xy})$ is illustrated, which would give six types of domains: $\pm x$, $\pm y$, and $\pm z$. If a domain structure does exist in $PrOs_4Sb_{12}$, then the μSR data indicate that the domains would likely be smaller (as scaled by λ) than in Sr_2RuO_4.[30]

In conclusion, magnetic scans of Sr_2RuO_4 and $PrOs_4Sb_{12}$ have been presented. No static magnetization remotely near the TRSB fields observed by μSR in both materials, or theoretical expectation for $p_x \pm i p_y$ order in Sr_2RuO_4, was observed.

Note added in proof. A scenario for chiral superconductivity in Sr_2RuO_4 where edge and domain wall currents are sharply reduced is discussed in Ref. 50. Superconductivity-related TRSB has also been observed in $LaNiC_2$.[51]

[1] A. P. Mackenzie and Y. Maeno, Rev. Mod. Phys. **75**, 657 (2003).

[2] P. J. Baker, R. J. Ormeno, C. E. Gough, Z. Q. Mao, S. Nishizaki, and Y. Maeno, Phys. Rev. B **80**, 115126 (2009).

[3] T. M. Riseman, P. G. Kealey, E. M. Forgan, A. P. Mackenzie, L. M. Galvin, A. W. Tyler, S. L. Lee, C. Ager, D. McK. Paul, C. M. Aegerter, R. Cubitt, Z. Q. Mao, T. Akima, and Y. Maeno, Nature (London) **396**, 242 (1998).

[4] G. M. Luke, Y. Fudamoto, K. M. Kojima, M. I. Larkin, B. Nachumi, Y. J. Uemura, J. E. Sonier, Y. Maeno, Z. Q. Mao, Y. Mori, and D. F. Agterberg, Physica B **289-290**, 373 (2000).

[5] E. D. Bauer, N. A. Frederick, P. C. Ho, V. S. Zapf, and M. B. Maple, Phys. Rev. B **65**, 100506(R) (2002).

[6] N. Nakai, M. Ichioka, and K. Machida, J. Phys. Soc. Jpn. **71**, 23 (2002).

[7] M.-A. Méasson, D. Braithwaite, G. Lapertot, J.-P. Brison, J. Flouquet, P. Bordet, H. Sugawara, and P. C. Canfield, Phys. Rev. B **77**, 134517 (2008).

[8] R. Vollmer, A. Faißt, C. Pfleiderer, H. v. Löhneysen, E. D. Bauer, P.-C. Ho, V. Zapf, and M. B. Maple, Phys. Rev. Lett. **90**, 057001 (2003).

[9] K. Grube, S. Drobnik, C. Pfleiderer, H. v. Löhneysen, E. D. Bauer, and M. B. Maple, Phys. Rev. B **73**, 104503 (2006).

[10] D. E. MacLaughlin, J. E. Sonier, R. H. Heffner, O. O. Bernal, B. L. Young, M. S. Rose, G. D. Morris, E. D. Bauer, T. D. Do, and M. B. Maple, Phys. Rev. Lett. **89**, 157001 (2002).

[11] L. Shu, D. E. MacLaughlin, W. P. Beyermann, R. H. Heffner, G. D. Morris, O. O. Bernal, F. D. Callaghan, J. E. Sonier, W. M. Yuhasz, N. A. Frederick, and M. B. Maple, Phys. Rev. B **79**, 174511 (2009).

[12] I. Bonalde, B. D. Yanoff, M. B. Salamon, D. J. Van Harlingen, E. M. E. Chia, Z. Q. Mao, and Y. Maeno, Phys. Rev. Lett. **85**, 4775 (2000).

[13] K. Deguchi, Z. Q. Mao, H. Yaguchi, and Y. Maeno, Phys. Rev. Lett. **92**, 047002 (2004).

[14] K. Deguchi, Z. Q. Mao, and Y. Maeno, J. Phys. Soc. Jpn. **73**, 1313 (2004).

[15] E. E. M. Chia, M. B. Salamon, H. Sugawara, and H. Sato, Phys. Rev. Lett. **91**, 247003 (2003).

[16] H. Kotegawa, M. Yogi, Y. Imamura, Y. Kawasaki, G.-q. Zheng, Y. Kitaoka, S. Ohsaki, H. Sugawara, Y. Aoki, and H. Sato, Phys. Rev. Lett. **90**, 027001 (2003).

[17] G. Seyfarth, J. P. Brison, M. A. Méasson, D. Braithwaite, G. Lapertot, and J. Flouquet, Phys. Rev. Lett. **97**, 236403 (2006).

[18] K. Ishida, H. Mukuda, Y. Kitaoka, K. Asayama, Z. Q. Mao, Y. Mori, and Y. Maeno, Nature (London) **396**, 658 (1998).

[19] W. Higemoto, S. R. Saha, A. Koda, K. Ohishi, R. Kadono, Y. Aoki, H. Sugawara, and H. Sato, Phys. Rev. B **75**, 020510(R) (2007).

[20] K. Ishida, Y. Kitaoka, K. Asayama, S. Ikeda, S. Nishizaki, Y. Maeno, K. Yoshida, and T. Fujita, Phys. Rev. B **56**, R505

(1997).

21 S. Kawasaki, K. Katayama, H. Sugawara, D. Kikuchi, H. Sato, and G. Q. Zheng, Phys. Rev. B **78**, 064510 (2008).

22 A. P. Mackenzie, R. K. W. Haselwimmer, A. W. Tyler, G. G. Lonzarich, Y. Mori, S. Nishizaki, and Y. Maeno, Phys. Rev. Lett. **80**, 161 (1998).

23 K. D. Nelson, Z. Q. Mao, Y. Maeno, and Y. Liu, Science **306**, 1151 (2004).

24 Jing Xia, Y. Maeno, P. T. Beyersdorf, M. M. Fejer, and A. Kapitulnik, Phys. Rev. Lett. **97**, 167002 (2006).

25 F. Kidwingira, J. D. Strand, D. J. van Harlingen, and Y. Maeno, Science **314**, 1267 (2006).

26 H. Kambara, S. Kashiwaya, H. Yaguchi, Y. Asano, Y. Tanaka, and Y. Maeno, Phys. Rev. Lett. **101**, 267003 (2008).

27 N. Okuda, T. Suzuki, Z. Q. Mao, Y. Maeno, and T. Fujita, Physica C **388-389**, 497 (2003).

28 S. Mukherjee and D. F. Agterberg, Phys. Rev. B **74**, 174505 (2006).

29 G. M. Luke, Y. Fudamoto, K. M. Kojima, M. I. Larkin, J. Merrin, B. Nachumi, Y. J. Uemura, Y. Maeno, Z. Q. Mao, Y. Mori, H. Nakamura, and M. Sigrist, Nature (London) **394**, 558 (1998).

30 Y. Aoki, A. Tsuchiya, T. Kanayama, S. R. Saha, H. Sugawara, H. Sato, W. Higemoto, A. Koda, K. Ohishi, K. Nishiyama, and R. Kadono, Phys. Rev. Lett. **91**, 067003 (2003).

31 M. Stone and R. Roy, Phys. Rev. B **69**, 184511 (2004).

32 M. Matsumoto and M. Sigrist, J. Phys. Soc. Jpn. **68**, 994 (1999); **68**, 3120 (1999).

33 C. Kallin and A. J. Berlinsky, J. Phys.: Condens. Matter **21**, 164210 (2009).

34 P. G. Björnsson, Y. Maeno, M. E. Huber, and K. A. Moler, Phys. Rev. B **72**, 012504 (2005).

35 J. R. Kirtley, C. Kallin, C. W. Hicks, E. A. Kim, Y. Liu, K. A. Moler, Y. Maeno, and K. D. Nelson, Phys. Rev. B **76**, 014526 (2007).

36 P. E. C. Ashby and C. Kallin, Phys. Rev. B **79**, 224509 (2009).

37 N. C. Koshnick, M. E. Huber, J. A. Bert, C. W. Hicks, J. Large, H. Edwards, and K. A. Moler, Appl. Phys. Lett. **93**, 243101 (2008).

38 M. E. Huber, N. C. Koshnick, H. Bluhm, L. J. Archuleta, T. Azua, P. G. Björnsson, B. W. Gardner, S. T. Halloran, E. A. Lucero, and K. A. Moler, Rev. Sci. Instrum. **79**, 053704 (2008).

39 Z. Q. Mao, Y. Maeno, and H. Fukazawa, Mater. Res. Bull. **35**, 1813 (2000).

40 V. O. Dolocan, C. Veauvy, F. Servant, P. Lejay, K. Hasselbach, Y. Liu, and D. Mailly, Phys. Rev. Lett. **95**, 097004 (2005).

41 K. Hasselbach, V. O. Dolocan, P. Lejay, and D. Mailly, Physica C **460-462**, 277 (2007).

42 V. Moshchalkov, M. Menghini, T. Nishio, Q. H. Chen, A. V. Silhanek, V. H. Dao, L. F. Chibotaru, N. D. Zhigadlo, and J. Karpinski, Phys. Rev. Lett. **102**, 117001 (2009).

43 V. O. Dolocan, P. Lejay, D. Mailly, and K. Hasselbach, Phys. Rev. B **74**, 144505 (2006).

44 C. D. Tesche and J. Clarke, J. Low Temp. Phys. **29**, 301 (1977).

45 J. S. Dodge, E. Kulatov, L. Klein, C. H. Ahn, J. W. Reiner, L. Miéville, T. H. Geballe, M. R. Beasley, A. Kapitulnik, H. Ohta, Y. Uspenskii, and S. Halilov, Phys. Rev. B **60**, R6987 (1999).

46 H. Bluhm, Phys. Rev. B **76**, 144507 (2007).

47 N. A. Logoboy and E. B. Sonin, Phys. Rev. B **79**, 094511 (2009).

48 M. W. Haverkort, I. S. Elfimov, L. H. Tjeng, G. A. Sawatzky, and A. Damascelli, Phys. Rev. Lett. **101**, 026406 (2008).

49 T. R. Abu Alrub and S. H. Curnoe, Phys. Rev. B **76**, 054514 (2007).

50 S. Raghu, A. Kapitulnik, S. A. Kivelson, arXiv:1003.2266 (unpublished).

51 A. D. Hillier, J. Quintanilla, and R. Cywinski, Phys. Rev. Lett. **102**, 117007 (2009).